

# A MeerKAT search for persistent radio sources towards twenty-five localised Fast Radio Bursts

L. L. Mfulwane<sup>1</sup>\*, J. O. Chibueze<sup>2,3</sup>, T. P. Letsele<sup>1</sup>, T. M. Nyambe<sup>1</sup>, C. Venter<sup>1,4</sup>, M. C. Bezuidenhout<sup>5,1</sup>, B. W. Stappers<sup>6</sup>, L. G. Spitler<sup>7</sup>, M. Caleb<sup>8,9,10</sup>, A. Deller<sup>11,8</sup>, J. A. S. Fortunato<sup>12</sup>, B. Cornejo<sup>13</sup>, F. Schüssler<sup>13</sup>, H. Ashkar<sup>14,15</sup>, F. Bradascio<sup>13,16</sup>, S. Kalita<sup>17,12</sup>, A. Kundu<sup>18,1</sup>, M. Kramer<sup>1,7,6</sup>, E. F. Keane<sup>19</sup>, A. Weltman<sup>12,20</sup>

<sup>1</sup>Centre for Space Research, North-West University, Private Bag X6001, Potchefstroom 2520, South Africa

<sup>2</sup>Department of Mathematical Sciences, University of South Africa, Cnr Christian de Wet Rd and Pioneer Avenue, Florida Park, 1709, Roodepoort, South Africa

<sup>3</sup>Department of Physics and Astronomy, Faculty of Physical Sciences, University of Nigeria, Carver Building, 1 University Road, Nsukka 410001, Nigeria

<sup>4</sup>National Institute for Theoretical and Computational Sciences (NITheCS), Potchefstroom, South Africa

<sup>5</sup>South African Radio Astronomy Observatory, Black River Park, 2 Fir Street, Observatory, Cape Town 7925, South Africa

<sup>6</sup>Jodrell Bank Centre for Astrophysics, Department of Physics and Astronomy, The University of Manchester, Oxford road, Manchester, M13 9PL, United Kingdom

<sup>7</sup>Max-Planck-Institut für Radioastronomie, Auf dem Hügel 69, D53121 Bonn, Germany

<sup>8</sup>ARC Centre of Excellence for Gravitational Wave Discovery (OzGrav), Hawthorn, VIC 3122, Australia

<sup>9</sup>CSIRO, Space and Astronomy, PO Box 1130, Bentley WA 6102, Australia

<sup>10</sup>Sydney Institute for Astronomy, School of Physics, The University of Sydney, NSW 2006, Australia

<sup>11</sup>Centre for Astrophysics and Supercomputing, Swinburne University of Technology, Hawthorn, VIC, 3122, Australia

<sup>12</sup>High Energy Physics, Cosmology and Astrophysics Theory (HEPCAT) Group, Department of Mathematics and Applied Mathematics,

University of Cape Town, Rondebosch, Cape Town, 7700, South Africa

<sup>13</sup>IRFU, CEA, Université Paris-Saclay, F-91191 Gif-sur-Yvette, France

<sup>14</sup>Laboratoire Leprince-Ringuet, École Polytechnique, CNRS, Institut Polytechnique de Paris, F-91128 Palaiseau, France

<sup>15</sup>Institute of Space Sciences (IEEC-CSIC), Campus UAB, Torre C5, 2a planta, 08193 Barcelona, Spain

<sup>16</sup>Université Paris-Saclay, CNRS/IN2P3, IJCLab, 91405 Orsay, France

<sup>17</sup>Astronomical Observatory, University of Warsaw, Al. Ujazdowskie 4, Warsaw 00478, Poland

<sup>18</sup>NASA Postdoctoral Program Fellow, Astrophysics Science Division, NASA Goddard Space Flight Center, Greenbelt, MD 20771, USA

<sup>19</sup>School of Physics, Trinity College Dublin, College Green, Dublin 2, D02 PN40, Ireland

<sup>20</sup>African Institute for Mathematical Sciences, 6 Melrose Road, Muizenberg, Cape Town, 7945, South Africa

Accepted XXX. Received YYY; in original form ZZZ

## ABSTRACT

The discovery of persistent radio sources (PRSs) associated with repeating fast radio bursts (FRBs) has shed light on the immediate environments and possible progenitors of these FRBs. The confirmed PRSs may support the theory that FRB progenitors are compact central engines, whilst the non-detections suggest diversity of FRB's local environment. We perform a subarcsecond-resolution MeerKAT search at 1.28 GHz on 25 well-localised FRB positions provided by ASKAP and MeerTRAP. We detect 14 radio sources and provide flux upper limits for 12 non-detections (both these numbers include a source that was detected during two epochs of observation, and not detected during one epoch, adding up to 26). One radio source shows variability as seen in flux variations over three epochs of observation. Archival optical data reveal excesses in the direction of 13 detected radio sources. Similarly for four sources in the X-ray band, with one possibly being a high-energy signature of a radio galaxy core. Since we cannot definitively classify our detected radio sources as PRSs, future high-resolution observations with e-MERLIN will be required to resolve the radio emission and pronounce on the presence of compact PRSs associated with the 14 detected sources presented here.

**Key words:** radio continuum: general – (transients:) fast radio bursts – radio continuum: transients

## 1 INTRODUCTION

Fast Radio Bursts (FRBs) are extremely bright, extragalactic radio sources that last for sub-milliseconds. The first FRB was discovered

by Lorimer et al. (2007) in the Murriyang (Parkes) data archive. More than 800 FRBs have been discovered since this first burst, of which 58 have been reported to repeat (The CHIME/FRB Collaboration et al. 2023; An et al. 2025; Wang et al. 2025). Therefore, there are two identified FRB populations, one-off FRBs and repeating FRBs. However, it is uncertain whether the majority or even all

\* mfulwane6@gmail.com

FRBs repeat on some cadence. Repeating FRBs are observed to produce multiple bursts over a short period of time, exhibiting a variety of burst energies. On the other hand, one-off FRBs are observed to produce only one burst. This suggests diverse emission processes and environments. A recent study by [Kirsten et al. \(2024\)](#) proposed that while the early studies suggest two populations indicate different environments, with longer observation time the burst energy distribution might suggest the possibility of the same environment under different physical conditions. Therefore, it is still not clear if the two population share the common origin.

Upon localisation of repeating FRBs such as FRB20121102A ([Chatterjee et al. 2017](#)), FRB20190520B ([Niu et al. 2022](#)), FRB20190417A ([Moroiyan et al. 2025](#)), and FRB20240114A ([Bruni et al. 2025](#)), compact persistent radio sources (PRSs) have been confirmed to be co-located with these FRBs at the milliarcsecond level. A PRS candidate associated with FRB20201124 was detected by [Ravi et al. \(2022\)](#) using Very Large Array (VLA) and [Bruni et al. \(2024\)](#) also detected the PRS with VLA observations at 15 and 22 GHz. The PRSs associated with FRB20121102A and FRB20190520B share several notable properties, including high radio luminosities and negative spectral indices, consistent with non-thermal synchrotron emission. Both are localised to dwarf host galaxies and are compact on milliarcsecond scales, suggesting emission from dense, confined regions. Furthermore, each exhibits variability in rotation measure (RM), indicating turbulent and magnetised local environment ([Chatterjee et al. 2017; Niu et al. 2022](#)). In contrast, the PRS associated with FRB20201124A shows a lower luminosity and a positive spectral index, consistent with a star-forming origin on sub-arcsecond scales ([Nimmo et al. 2022; Bruni et al. 2024](#)). Similarly, the PRS associated with FRB20190417A shows low luminosity and a negative spectral index; it is localised within a star-forming dwarf galaxy and is compact at milliarcsecond scale, also suggesting a confined environment ([Ibik et al. 2024; Moroiyan et al. 2025](#)). The PRSs exhibit luminosities that range from  $L_\nu \approx 10^{27} - 10^{29}$  ergs  $\text{s}^{-1}$   $\text{Hz}^{-1}$  and are usually spatially offset from the centre of their host galaxy. [Yang et al. \(2020\)](#) proposed a relation between the PRS luminosity and the FRB's RM, suggesting that highly luminous PRSs are consistent with larger RMs. The emission from the compact radio source can persist on timescales of days, months, to years. Therefore, PRSs are compact radio sources with a long lifespan that are not active galactic nuclei (AGNi), but brighter than the galaxy's local star formation signature ([Ibik et al. 2024](#)). However, so far no PRS has been associated with a one-off FRB; therefore, this suggests a diversity of FRB progenitors or different emission mechanisms ([An et al. 2025](#)).

There are several models addressing the FRB progenitor question, most of which are linked with young and rapidly rotating neutron stars (isolated ones or merging ones; [Margalit et al. 2019](#)). [Totani \(2013\)](#); [Yamasaki et al. \(2018\)](#) proposed that the progenitor may be a merger between binary neutron stars. [Popov & Postnov \(2013\)](#) proposed hyperflares and giant flares from magnetars, while [Kashiyama et al. \(2013\)](#) suggested white dwarfs as the progenitor. A leading theory is a single central engine (magnetar), powering both the FRB and the PRS (magnetar wind nebula). For example, [Margalit et al. \(2019\)](#) proposed persistent emission as a result of a magnetar nebula, suggesting that the emission is powered by the relativistic electrons and magnetic fields energised by magnetar flares and leading to nebular expansion. Another model is the ultra-relativistic pulsar wind nebula that sweeps up its surrounding medium, with FRBs repeatedly produced via several mechanisms ([Dai et al. 2017](#)).

The presence of a PRS coinciding with an FRB offers crucial clues about the PRS progenitor. Probing the immediate environments of PRSs enables us to explore the mechanisms responsible for the

persistent emission and better understand whether the associated PRSs are a universal feature of all repeating FRBs or are linked to specific progenitor systems. [Law et al. \(2022\)](#) mentioned that PRSs could be associated with one-off FRBs, as the association of FRB / PRS is unclear. Given the probable diversity of FRB environments, a detailed study of several FRBs will be essential to understand their emission mechanisms and progenitor channels.

[An et al. \(2025\)](#) made an argument that the proposed diversity in FRB progenitors may rather be a result of observational limitations instead of physical intrinsic differences; i.e., one-off FRBs could be associated with faint PRSs which are below the sensitivity threshold. Therefore, there may be an evolving progenitor: the active FRB bursts and luminous PRS require a young and energetic progenitor, while one-off FRB with a fainter PRS requires an evolved, older progenitor. To determine if the hypothesis that one-off FRBs could be generated by evolved progenitors resulting in faint PRS holds, or if PRSs are exclusive to repeating FRBs, it is necessary to conduct an extensive PRS search using a substantial sample of well-localised one-off FRBs. Therefore, to elucidate the nature of FRB progenitors and the characteristics of the environment, and to address the question whether PRSs are solely associated with repeaters or also with one-off FRBs, we aim to search for PRSs associated with one-off FRBs.

Finding a strong association between an FRB and a PRS is not straightforward. An association is deemed reliable for  $\sim 20$  arcseconds localisations ([Nimmo et al. 2022; Ibik et al. 2024](#)). However, other processes not related to the FRB/PRS association can also generate the persistent radio emission. The most significant among these is star-formation-related radio emission from the host galaxy due to synchrotron emission ([Ibik et al. 2024](#)). The PRS can be distinguished from that of other persistent radio emission based on its angular size and/or spectral index, but this requires multi-frequency observations as well as observations at different angular scales ([Marcote et al. 2017; Bhandari et al. 2023; Dong et al. 2024](#)).

The primary purpose of this work is to provide a finder chart for PRSs using the MeerKAT telescope. We search for PRS candidates that are located near FRB positions that have been well localised by the Australian SKA Pathfinder (ASKAP) telescope and MeerTRAP. Our detected radio flux provides an upper limit for the potential PRS flux (due to possible contamination from the host galaxy emission) and can support high angular resolution and/or high-frequency follow-up observations. In addition, we searched for archival data in the optical and X-ray bands in different catalogs in the direction of our detected radio sources. This paper is structured as follows: Section 2 discusses observations and data reduction; Section 3 describes the radio continuum detection. Section 4 discusses our new source detections, and lastly Section 5 presents the conclusions and future work.

## 2 OBSERVATIONS AND DATA REDUCTION

### 2.1 FRB Sample

To search for PRSs candidates using the MeerKAT telescope, we used a sample consist of 25 one-off FRB positions, localised by ASKAP/CRAFT and MeerTRAP (see Section 5). In addition to selecting well-localised sources, the selection criteria of these FRBs were not strict as such. The selected sample exhibited lower DMs and redshifts, increasing the likelihood of detecting PRSs. In addition, radio bursts that had repeater-like properties were also taken into consideration, because only repeaters seem to be associated

with PRSs. Our MeerKAT observations have been obtained based on 2021, 2022, and 2023 open time proposals (SCI-20210212-CV-01, SCI-20220822-CV-01, SCI-20230907-CV-01, respectively, see Chibueze et al. 2022).

## 2.2 MeerKAT Observations

The MeerKAT radio telescope is a 64-antenna interferometer array that is located in the northern Karoo desert. Each dish is a Gregorian parabolic surface with an effective diameter of 13.5 metres. Of the 64 dishes, 48 are located within a 1 km radius around the array’s inner core, and the remaining 16 are spread outward up to 8 km. The MeerKAT array’s smallest and longest baselines are 29 m and 8 km, respectively. The angular scales range from 5 arcseconds to 27 arcminutes at the central frequency of the L-band (1283 MHz). MeerKAT was used to observe different FRB positions with 90 minutes of on-source integration time, and a phase calibrator observed for 2 minutes for every 15 minutes on the targeted FRB position. The observation period is repeated for each epoch of these FRB fields at the L-band (856–1712 MHz). Data were reduced using oxkat3, a semi-automated MeerKAT data analysis pipeline (Heywood 2020).

## 2.3 Calibration and Imaging

The oxkat3 pipeline utilises radio interferometric data reduction software that is publicly available. The pipeline provides reduced and calibrated visibility data, continuum images, and diagnostic plots as the final data. In addition, the customary configuration includes flagging, cross-calibration, and self-calibration processes. In the case of the flagging process, the low-gain bandpass edges, which are 856–880 MHz and 1658–1800 MHz, are flagged on all baselines. The location of the Galactic neutral hydrogen line (1419.8–1421.3 MHz) is also flagged to remove line contamination as a result of the continuum imaging process. The radio frequency interference (RFI) is also flagged out in regions with baselines shorter than 600 m. Other RFI that might have impacted the data are flagged using case tasks such as RFLAG and TFCROP for the calibrators and the TRICOLOR package for the target fields (McMullin & et al. 2007).

In the case of cross-calibration, oxkat uses casa tasks, which includes standard steps such as setting the flux scale and deriving corrections for residual delay calibration, bandpass, and time-varying gain (McMullin & et al. 2007). After all corrections are applied on target fields, every five consecutive frequency channels are averaged. Then only the calibrated visibilities from the field target are extracted to obtain the science target. The target data are deconvolved and imaged using the WSClean imager, which comprises of the multiscale and wideband deconvolution algorithms (which allows better imaging of diffuse emission present in our fields). The full bandwidth is divided into 10 subbands, each with a bandwidth of 82 MHz. Then deconvolution is performed in each subband images.

WSClean generates the multi-frequency synthesis (MFS) map (Oftringa et al. 2014), which is a full bandwidth map consisting of a central frequency of 1283 MHz in joined-channel deconvolution mode. Each of the 10 subbands is deconvolved with an initial high mask of  $20\sigma_{\text{rms}}$  using the auto masking function provided by WSClean, where  $\sigma_{\text{rms}}$  is the root mean square noise. After the deconvolution process, an artefact-free model of the target field is generated for the self-calibration process. In the final iteration of imaging, the masking threshold is reduced to  $3\sigma_{\text{rms}}$ . For self-calibration, the oxkat pipeline uses tasks from the Cubical software (Kenyon et al. 2018). The flux

densities reported in this work were measured using the casa task *imfit*<sup>1</sup>.

## 3 RESULTS

We report on a search for PRS candidates associated with 25 FRB positions (see Appendix A1) using MeerKAT. These are one-off FRBs, which have been localised by ASKAP and MeerTRAP to an arcsecond position. Of the 25 FRBs, there are multi-epoch observations of some sources, which should have resulted in a total of 39 FRB fields. However, due to a calibration failure of one field, we have 38 FRB fields in total. Figures 1, 2, 3, and 4 show the 38 FRB MeerKAT fields we searched for PRS candidates. The ASKAP / MeerTRAP FRB position is indicated by a cyan circle, and white contours represent MeerKAT radio continuum emission.

### 3.1 MeerKAT detection of PRS candidates

Out of 25 FRB positions (see Appendix A1), we detect radio emission coinciding with 14 FRB positions (Figures 3 and 4), with the intensity  $\geq 3\sigma_{\text{rms}}$  noise level. There are a total of 21 fields with detections when follow-up epochs are included. Specifically, the FRB20220501C fields, which have three follow-ups, show flux variability and a source is only detected in two observational epochs (and not detected in one epoch). The peak intensity and flux density for each detection are obtained by performing a 2D Gaussian fit of an ellipse region surrounding the detected continuum emission. Also, the flux density uncertainties were obtained and the values are reported in Table 1. Table 4 presents the angular separations between each FRB and its associated radio source. Eftekhari & Berger (2017) investigated FRB–host galaxy associations as a function of apparent magnitude and localisation region, applying their methodology to several radio facilities, including the MeerKAT telescope. Their analysis showed that MeerKAT localisation capabilities ranges to  $\sim 2''$ – $10''$ . In our detection sample, 13 of the 14 radio detections are coincide with corresponding FRB positions within the expected uncertainties. One candidate which exhibits a significantly large offset, indicates poor positional coincidence between FRBs and the corresponding radio sources, despite an apparent coincidence upon visual inspection. Such a discrepancy may arise from incorrect centroiding, due to shifted source centroids caused by complex morphologies thus the position may not reflect the centroid of the relevant physical association. Consequently, we do not completely rule out the plausibility of these associations, but we regard them with caution. The physical origin of the detected radio emission remains uncertain; therefore, follow-up observations with a higher angular resolution will be essential for identifying the true nature of the emission.

### 3.2 MeerKAT non-detection of PRS candidates

We could not detect any radio emission coinciding with the other 11 FRB positions, and additionally also for one epoch of observation

<sup>1</sup> A detection in a MeerKAT image is defined as a signal with a significance of  $\geq 3\sigma_{\text{rms}}$ . Accordingly, a region is carefully drawn along the inside  $3\sigma_{\text{rms}}$  contour line of the target source using CASA Viewer to obtain an accurate flux. The CASA *imfit* task is subsequently used to perform a Gaussian fit. This method yields best-fit parameter values, including peak flux density, integrated flux density, position (RA,DEC), and source size (major/minor axes, position angle) of the target source. In addition, the corresponding errors for each fitted parameter are provided in Table 1.

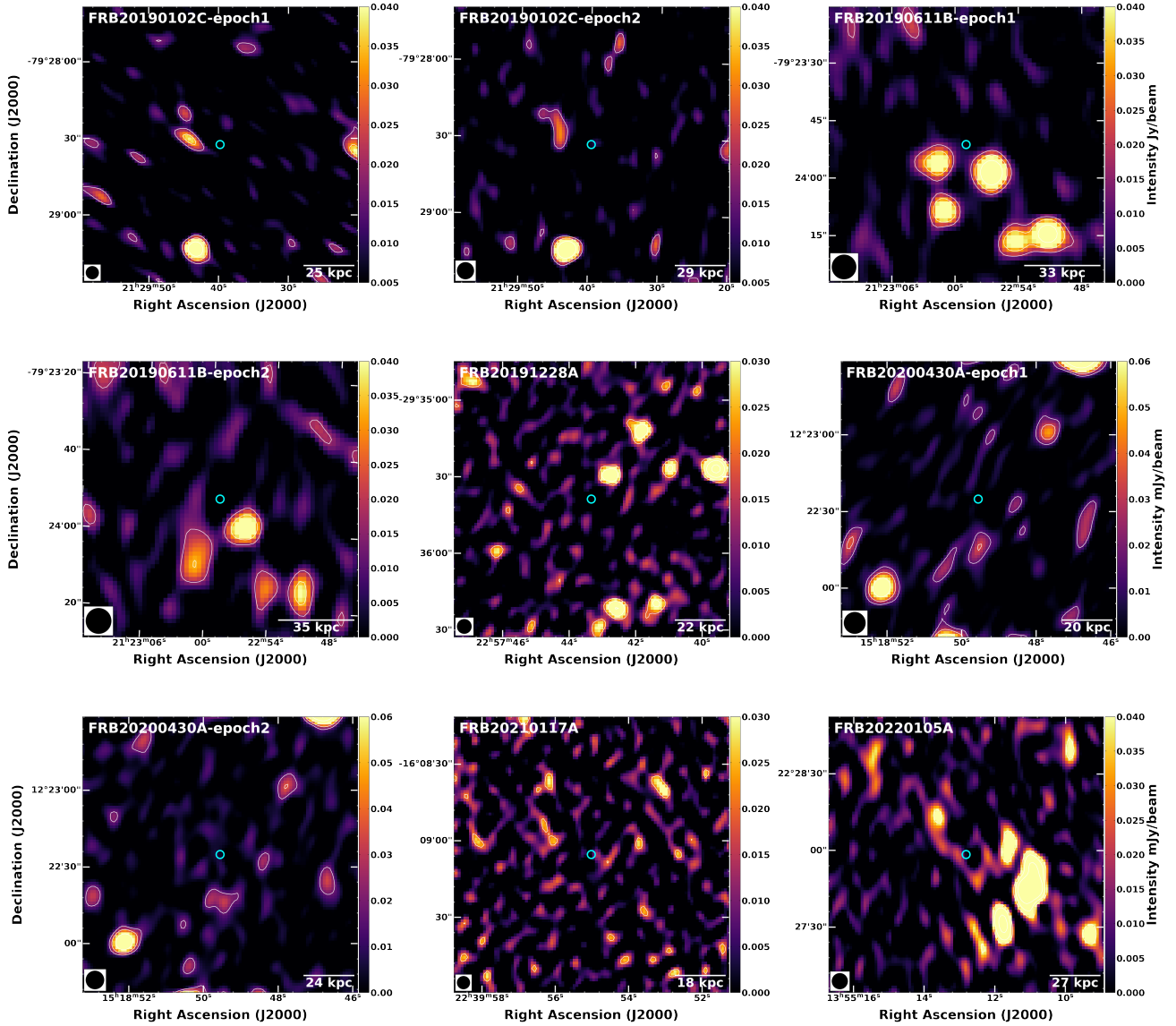


**Figure 1.** Non-detections by MeerKAT. The cyan circle indicates the position of the ASKAP/MeerTRAP FRB. White contours corresponding to 3, 6, 12, 24 times the rms of the image represent non-associated continuum radio emission. The black circle in the bottom left corner represents the beam size of MeerKAT in each case. For sources that were observed for more than one epoch, we indicate the epoch as part of the FRB name.

on FRB20220501C. Considering multiple epochs of observation, this should give a total 18 FRB fields. Of these, there are 17 non-detections with 1 calibration failure. Given that each FRB field has a residual image, the  $\sigma_{\text{rms}}$  noise of each field is obtained. We therefore compute the  $3\sigma$  intensity upper limit based on the  $\sigma_{\text{rms}}$  and these values are reported in Table 2.

### 3.3 Multi-wavelength data for potential PRSs

#### 3.3.1 Optical counterparts

We searched for optical counterparts from the Panoramic Survey Telescope and Rapid Response System (Pan-STARRS) catalog (PS1) (Flewelling et al. 2020) for the *g*-band; and Dark Energy Spectroscopy Instrument (DESI), data release 10 (DR10) Legacy Imaging Survey photometric catalog (Dey et al. 2019) for the *grz*-bands. We

found that optical counterparts spatially coincide with only 13 detected radio sources, as shown in Figures A1 and A2 and there is no optical source spatially coinciding with FRB20210912A. The relevant citations to detailed studies on the optical sources are listed in Table 3. A more detailed study towards the positions of FRB20220501, FRB20221106, FRB20220918, and FRB20210912A will be done in an upcoming work (Mfulwane et al., in prep). The Pan-STARRS and DESI catalogs are used to verify that the optical sources are not characterised as probable stars and to visually inspect the offsets between the optical and radio sources. Figures A1 and A2 also indicate the FRB position with respect to the optical source, and whether the FRB location is offset from the optical position. By visually inspecting the morphology of detected radio and optical sources, it can be seen that most the radio sources are large-scale structures, probably associated with the host galaxy. Also to confirm the coincidence between the radio and optical sources, the positional angular offsets ( $\Delta\theta$ ) are listed

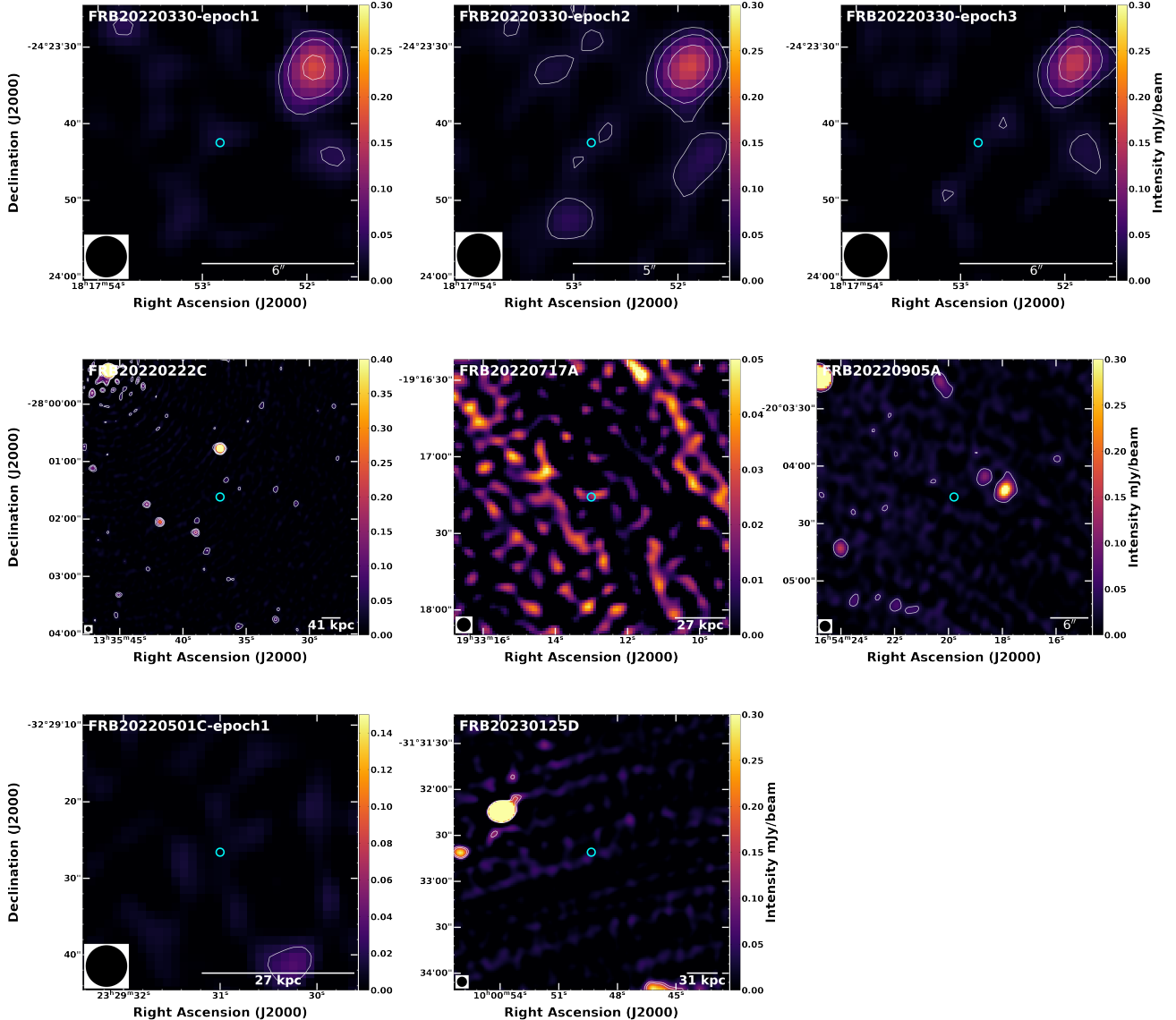


**Figure 2.** Non-detections by MeerKAT. The cyan circle indicates the position of the ASKAP/MeerTRAP FRB. White contours corresponding to 3, 6, 12, 24 times the rms of the image represent non-associated continuum radio emission. The black circle in the bottom left corner represents the beam size of MeerKAT in each case. For sources that were observed for more than one epoch, we indicate the epoch as part of the FRB name.

in Table 4, and some of our optical sources are resolved. We adopted the radio-optical positional offset threshold  $\Delta\theta \leq 0.5''$  for the radio source to be consistent with an AGN (Orosz & Frey 2013; Ibik et al. 2024). For a single-component radio source the radio-optical offset threshold required ranges within  $\sim 0.5'' - 1.0''$  (Magliocchetti & Maddox 2002; Heywood et al. 2022). In the case of a faint source, a threshold of  $\sim 2''$  is applied, while faint and slightly extended radio sources may require the threshold of  $\sim 3''$  (Lindsay et al. 2014; Whittam et al. 2023). Offsets larger than  $3''$  are likely due to unresolved multiple sources or complex morphology (see FRB20181112 in Figure A2); visual inspection shows that the radio and the optical emission coincide, thus suggesting large offsets arise from uncertainty of the centroid positions. In the case of FRB20210912, there is no optical counterpart found in the archive, thus radio-optical positional offsets are not calculated. Three of our sources are may be consistent with AGN. The redshift of our detected sample of radio

sources range from  $z = 0.0469 - 0.491$ , corresponding to projected sizes probed by MeerKAT that range from  $\sim 5 - 40$  kpc.

### 3.3.2 X-ray counterparts

We searched *Chandra* (Weisskopf & et al. 2002) and *Swift* (Burrows et al. 2005) catalogs for X-ray counterparts to the detected radio sources. Of the 14 FRB detected sources, only one plausible X-ray counterpart was found, as shown in Figures A3 and A4, subject to follow-up analyses. Confirmed X-ray counterparts would indicate the operation of non-thermal processes. Future observations or deeper searches may reveal X-ray emission for the other radio sources.

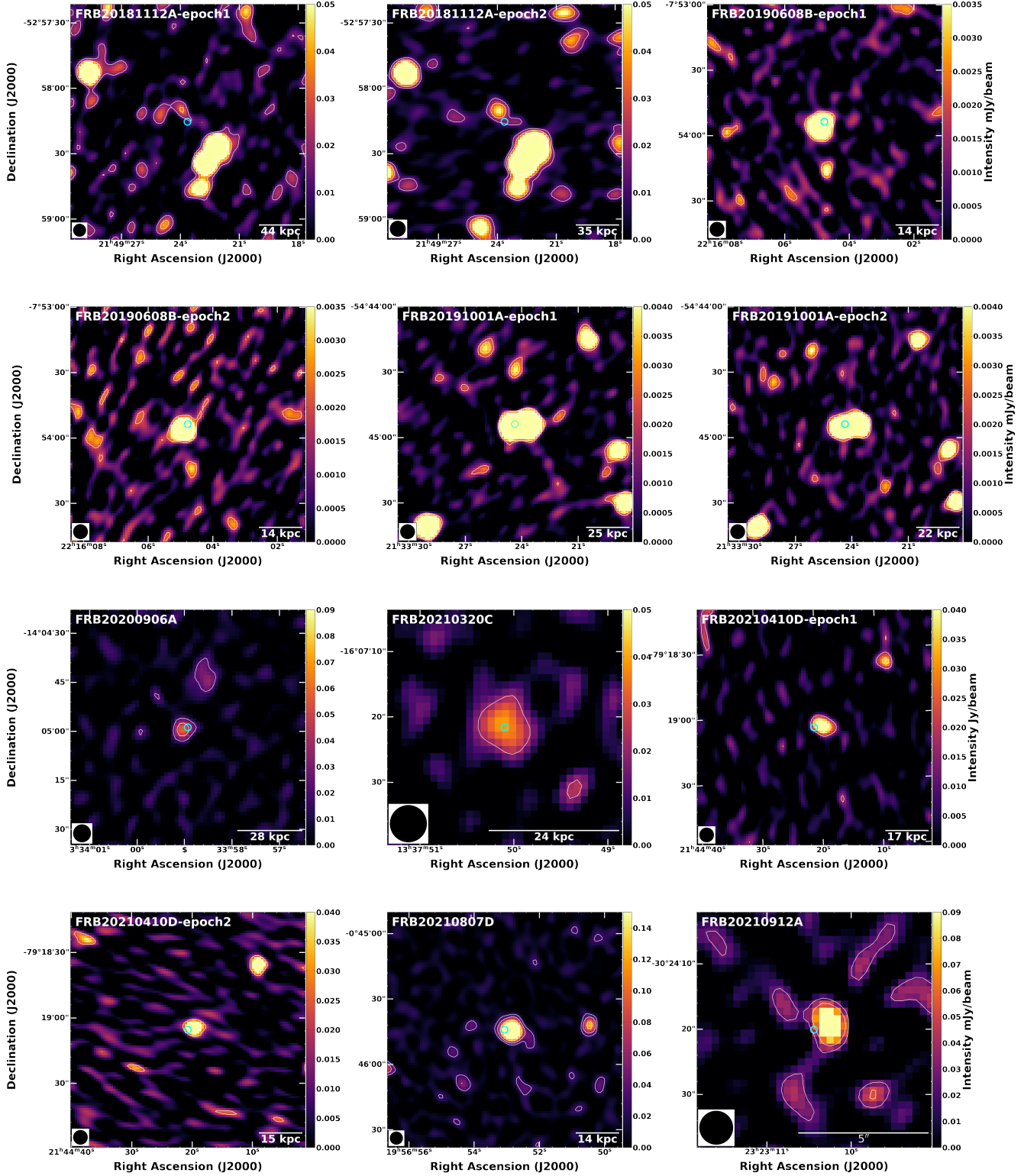


**Figure 3.** MeerKAT images of various FRB sources at different angular scales. The cyan circle indicates the position of the FRB. White contours corresponding to 3, 6, 12, 24  $\times$  the respective rms (see Table 1) of the images represent continuum radio emission coincident with the FRB position. The black circle in the bottom left corner represents the beam size of MeerKAT. For sources that were observed for more than one epoch, we indicate the epoch as part of the FRB name.

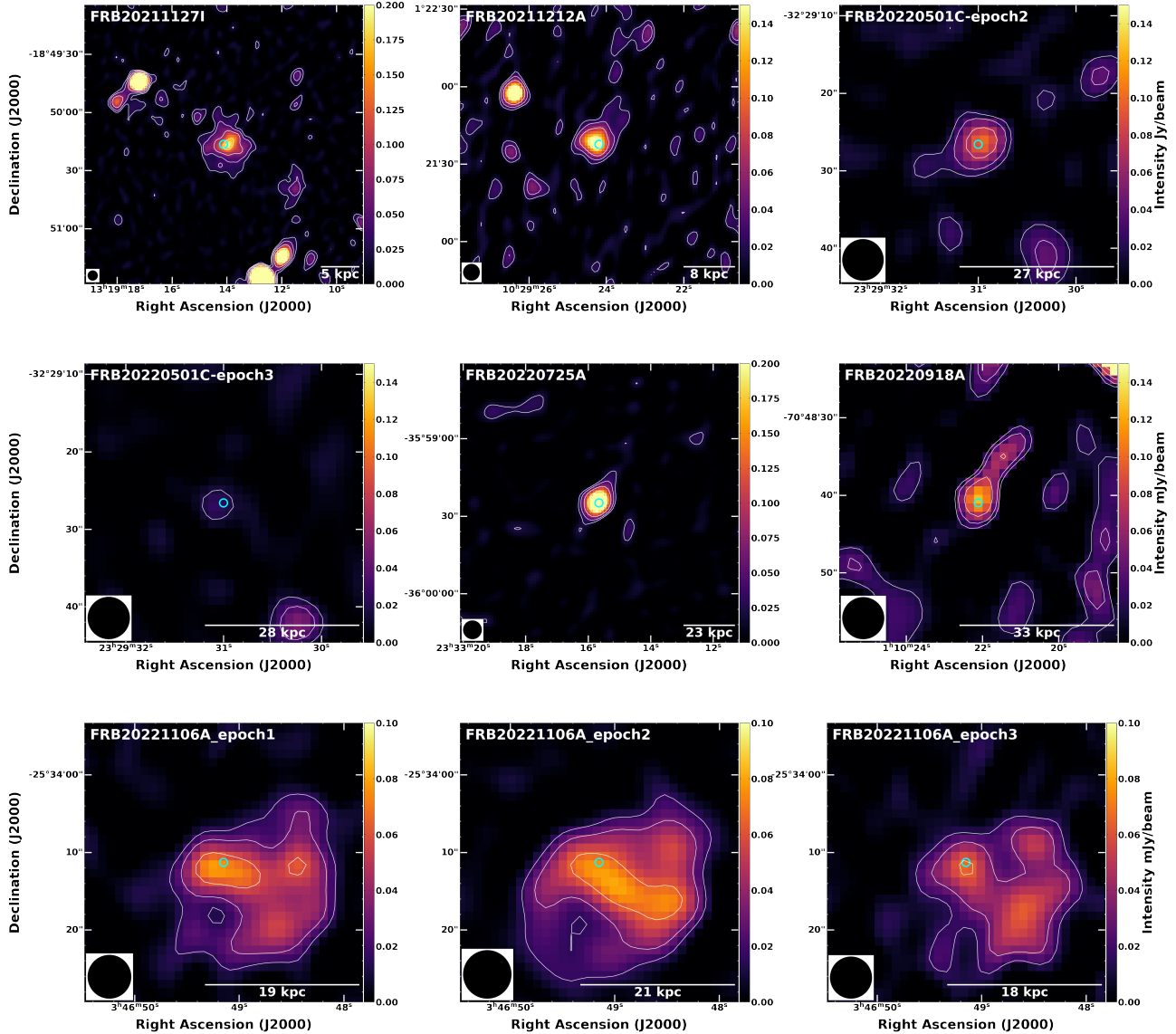


**Figure 4.** MeerKAT images of various FRB sources at different angular scales. The cyan circle indicates the position of the FRB. White contours corresponding to 3, 6, 12, 24  $\times$  the respective rms (see Table 1) of the images represent continuum radio emission coincident with the FRB position. The black circle in the bottom left corner represents the beam size of MeerKAT. For sources that were observed for more than one epoch, we indicate the epoch as part of the FRB name.

### 3.3.3 Cross-check of multi-wavelength counterparts

To ensure the robustness of the multi-wavelength associations, we performed an independent cross-check of the FRB fields within a radius of 15'' from each MeerKAT detection. This verification used two additional datasets: Wide-field Infrared Survey Explorer (WISE) (Wright et al. 2010) mid-infrared imaging, W1 and W2 bands, and Gaia DR3 astrometric catalogs (Brown et al. 2021). The procedure confirmed all optical identifications reported above and revealed a few cases where bright foreground stars are present within the search region, as identified through Gaia parallax and proper motion measurements. In particular, in the fields of FRB20220501C, FRB2018112A, and FRB20210807D, Gaia detects nearby stars located close to the radio position. While these stars are not proposed as counterparts to the FRBs, their presence highlights the possibility

of contamination in the optical or infrared images, and was taken into account when visually inspecting the multi-wavelength data.

### 3.4 Radio-to-optical (RO) ratio calculation

Since most of our MeerKAT detected radio sources are not offset from their likely optical counterparts (hosts) and seem to be consistent with large-scale structures, we used the RO ratio as a diagnostic metric to check for “radio excess” above the expected emission due to star formation, as given in Table 5. A significant excess radio emission could signal the presence of non-thermal radio emission (a PRS). The RO ratio is calculated as  $RO = \log_{10}(S_{1.2\text{GHz}}/S_{\text{optical}})$ , where  $S_{1.2\text{GHz}}$  is the flux density of MeerKAT radio sources at 1.2 GHz in Jansky and  $S_{\text{optical}}$  is the optical flux density in Jansky. The optical flux density is calculated as  $S_{\text{optical}} = 3631 \times 10^{-0.4m_r}$  (Afonso et al.

2005; Ibik et al. 2024), where  $m_r$  is the published AB  $r$ -band magnitude of the host galaxies. We adopted the threshold used by Eftekhari et al. (2021); Ibik et al. (2024), where an RO ratio  $< 1.4$  is consistent with pure star formation and an RO ratio  $> 1.4$  is consistent with other radio emission such as those related to AGN activities, pulsar wind nebulae, hypernebulae, supernova remnants, gamma-ray bursts, etc. For example, Ibik et al. (2024) found an RO ratio of the PRS associated with FRB20121102A of  $\sim 2.9$  using  $250 \mu\text{Jy}$  at 1.63 GHz and  $\sim 1.7$  using  $258 \mu\text{Jy}$  at 1.5 GHz for the PRS associated with FRB20190520B (Ibik et al. 2024), which imply radio emissions that are not solely due to star formation but could be linked to AGN or PRS emission. Of the 14 detected sources, we performed the calculation for only nine sources for which we could find the published AB-magnitudes. For the sources for which we could perform the calculation, the ratio is  $< 1.4$  suggesting that the radio emission is consistent with pure star-formation (see Table 5).

## 4 DISCUSSION

Of the 38 FRB target fields reported in this paper, we have detected continuum radio emission toward 14 unique FRB positions (a total of 21 FRB fields for multiple observational epochs). There is no detection toward 11 FRB unique positions (a total of 18 FRB fields for multiple epochs). These non-detections might suggest that the radio sources have faded away (quiescent source), or that they are too faint for MeerKAT to detect. Therefore, a radio flux upper limit for each field was derived.

For all 14 detected radio sources, we searched for optical counterparts in archival catalogues and found 13; of these, 11 optical counterparts have previously been studied in detail (Table 3). Given the resolution of MeerKAT telescope, we detected unresolved radio emission and by visual inspection, our radio sources overlap with these optical sources. In addition, the morphology of the detected radio sources seems to resemble that of the corresponding optical sources, e.g., the radio emission structure of FRB20191001A is symmetric with respect to the two optical galaxies. Therefore, the detected radio sources are consistent with the large-scale optical sources instead of compact PRSs. Therefore, we applied a diagnostic method to check if the continuum radio emission is consistent with star formation or if there is an excess radio emission (see Table 5) resulting from sources such as AGN or PRSs. For the nine sources for which we could do the calculations, the detections are consistent with star formation ( $RO < 1.4$ ). These results may imply that the continuum emission from star formation might be dominating over any faint PRS signal that might exist. In addition, the luminosity of the MeerKAT radio sources range from  $2.7 \times 10^{28} - 9.4 \times 10^{29}$   $\text{erg s}^{-1} \text{Hz}^{-1}$ , to check if the luminosity of these sources are consistent with the PRSs detected. Thus, the luminosities seem to fall within the range, therefore high resolution observations are required to confirm the nature of these sources. A deep targeted search with a high-resolution radio telescope is necessary to elucidate the existence of compact PRSs, resolving them from the radio emission detected here (Mfulwane et al., in prep). The lack of offset between optical and radio means we cannot exclude the possibility of an AGN origin.

<sup>2</sup> Of all the radio sources detected, only the radio source associated

with FRB20220501C shows variability behaviour in the radio band. The optical counterpart associated with this source is not classified. No comparative analysis was performed for the X-ray data, as no X-ray counterparts were detected at the relevant positions, except for a single case where it is uncertain if it is a real detection.

## 5 CONCLUSIONS AND FUTURE WORK

We conducted a search for continuum radio emission using MeerKAT towards 25 FRBs localised by ASKAP and MeerTRAP. This study is a precursor for searching and identifying potential PRS candidates. Of the 25 FRB positions, we detected radio sources for 14 unique FRB positions and the flux densities of these detected sources have been determined. In the case of FRB20220501C field that was observed for three epochs, we found no detection in the first epoch, but made a detection in the second and third epochs, suggesting flux variability on day-timescales. This variability is intrinsic or due to scintillation effects. We furthermore found potential optical counterparts for 13 radio sources, and a possible X-ray counterpart for only one source. Most of the optical counterparts found in the archival catalogues are classified as galaxies (FRB host galaxies). There are detailed studies in the literature for most of these optical sources, except for optical sources coinciding with the radio emission in three FRB fields, namely, FRB20220501C, FRB20221106A, and FRB20220918A. Therefore, no identification can be made regarding these three radio sources. One may also study the unknown hosts of these three FRBs at sub-millimeter wavelengths.

Our detected radio sources are unresolved, overlap with the optical sources, and furthermore their morphology have some resemblance to the optical ones. This may imply that we observed the large-scale (host galaxy) emission from star formation instead of PRSs. Indeed, we found that the radio emission is consistent with star formation within the host using the RO ratio, and there is no sign of excess emission (see Table 5) resulting from sources such as PRSs. We therefore conclude that either there is no PRS, or a faint PRS may be embedded within the radio emission resulting from star formation in the region. In order to confirm the existence of a compact PRS, deep, targeted observations using the high-resolution enhanced Multi-Element Remote-Linked Interferometer (e-MERLIN) telescope are required with the aim of disentangling the observed radio sources from compact PRSs and, if detected, determine the size of the compact PRSs, check for variability and spectral shape, constrain the flux density, and search for very high energy counterparts with the High Energy Stereoscopic System (H.E.S.S.).

## ACKNOWLEDGEMENTS

This paper utilises MeerKAT L-band observational data from 2021, 2022, and 2023 open-time proposals (SCI-20210212-CV-01, SCI-20220822-CV-01, SCI-20230907-CV-01, respectively). The South African Radio Astronomy Observatory, a facility of the National Research Foundation, operates the MeerKAT telescope. The Inter-University Institute for Data Intensive Astronomy (IDIA) visualisation lab <https://idia.ac.za/citing-idia-ilifu-in-publications/> is used to for this work. IDIA is a partnership of the University of Cape Town, the University of Pretoria, the University of the Western Cape and

<sup>2</sup> Our logic is as follows. The radio emission may trace the AGN activity, while the optical emission traces the host galaxy (star formation) emission. When there is a large radio-optical offset  $> 0.5''$ , the radio emission could be due to other processes such as star formation. On the other hand, a small radio-optical offset, can imply that the radio emission originates from the

same region as the optical nucleus, suggesting an AGN origin. Thus, the radio emission does not originate from star formation but from AGN-driven processes such as synchrotron emission from jets or a compact core

**Table 1.** Detection of continuum radio emission.

Source name	Observation date	R.A.(J2000)	Dec.(J2000)	Synthesised beam (mJy beam <sup>-1</sup> )	rms (mJy beam <sup>-1</sup> )	Peak Flux mJy beam <sup>-1</sup>	Maj×Min axis	Pos. Angle	Int. Flux mJy
FRB20181112A	19-Apr-2021	21:49:23.63	-52:58:15.4	7''.304×7''.304	0.0047	0.0371	5''.63×5''.15	45°	0.0202 ± 0.0091
FRB20181112A	03-Sep-2021	21:49:23.63	-52:58:15.4	5''.940×5''.940	0.0054	0.0219	5''.64×3''.55	34°	0.0124 ± 0.0061
FRB20190608B	10-Apr-2021	22:16:04.77	-07:53:53.7	6''.621×6''.621	0.000581	0.0170	7''.45×6''.87	146°	0.0199 ± 0.0014
FRB20190608B	02-Sep-2021	22:16:04.77	-07:53:53.7	6''.465×6''.465	0.000587	0.0174	7''.36×6''.78	82°	0.0205 ± 0.0015
FRB20191001A	10-Apr-2021	21:33:24.41	-54:44:53.9	6''.831×6''.831	0.00057	0.0571	11''.97×6''.91	98°	0.1013 ± 0.0110
FRB20191001A	02-Sep-2021	21:33:24.41	-54:44:53.9	5''.914×5''.914	0.00067	0.0462	11''.25×5''.63	98°	0.0837 ± 0.0130
FRB20200906A	18-Jan-2023	03:33:58.93	-14:04:58.8	5''.476×5''.476	0.007175	0.0521	5''.43×5''.00	134°	0.0473 ± 0.0069
FRB20210320C	19-Feb-2023	13:37:50.10	-16:07:21.6	5''.698×5''.698,	0.006837	0.0317	7''.49×6''.20	27°	0.0454 ± 0.0069
FRB20210410D	05-Sep-2021	21:44:20.7	-79:19:05.5	6''.723×6''.723	0.0053	0.0546	8''.22×5''.87	63°	0.0583 ± 0.0080
FRB20210410D	14-Feb-2023	21:44:20.7	-79:19:05.5	5''.880×5''.880	0.0076	0.0714	6''.09×5''.24	98°	0.0659 ± 0.0074
FRB20210807D	23-Dec-2022	19:56:53.07	-00:45:44.1	5''.997×5''.997	0.0089	0.4699	6''.40×6''.11	60°	0.5110 ± 0.0260
FRB20210912A	22-Dec-2022	23:23:10.44	-30:24:20.1	5''.171×5''.171	0.0084	0.1318	5''.16×3''.76	18°	0.0957 ± 0.0106
FRB20211127I	18-Jan-2023	13:19:14.12	-18:50:16.5	5''.299×5''.299	0.0066	0.1495	9''.78×7''.91	120°	0.4118 ± 0.0800
FRB20211212A	15-Dec-2022	10:29:24.19	+01:21:37.6	6''.526×6''.526	0.0058	0.1596	8''.26×7''.79	63°	0.2413 ± 0.0360
FRB20220501C	25-Nov-2023	23:29:31.00	-32:29:26.60	5''.388×5''.388	0.0056	0.0899	4''.71×4''.03	136°	0.0588 ± 0.0130
FRB20220501C	26-Nov-2023	23:29:31.00	-32:29:26.6	5''.480×5''.480	0.0053	0.0609	5''.95×5''.72	98°	0.0691 ± 0.0038
FRB20220725A	09-Nov-2023	23:33:15.65	-35:59:24.9	7''.268×7''.268	0.0072	0.3506	8''.11×6''.45	147°	0.3473 ± 0.0370
FRB20220918A	16-Nov-2023	01:10:22.11	-70:48:41.0	5''.433×5''.433	0.0058	0.0859	3''.36×2''.21	163°	0.0216 ± 0.0025
FRB20221106A	21-Nov-2023	03:46:49.15	-25:34:11.3	5''.649×5''.649	0.0048	0.0446	14''.30×5''.33	78°	0.1065 ± 0.0480
FRB20221106A	05-Dec-2023	03:46:49.15	-25:34:11.3	6''.264×6''.264	0.0054	0.0557	18''.22×8''.37	67°	0.2167 ± 0.0670
FRB20221106A	20-Jan-2024	03:46:49.15	-25:34:11.3	5''.452×5''.452	0.0053	0.0270	20''.59×5''.39	55°	0.1096 ± 0.0700

**Table 2.** Sources for which continuum radio emission is not detected.

Source name	Observation date	R.A.(J2000)	Dec.(J2000)	Synthesised beam	rms mJy beam <sup>-1</sup>	Upper limit mJy beam <sup>-1</sup>
FRB20190102C	10-Apr-2021	21:29:39.76	-79:28:32.5	5''.709×5''.709	0.0054	< 0.0162
FRB20190102C	05-Sep-2021	21:29:39.76	-79:28:32.5	6''.723×6''.723	0.0055	< 0.0164
FRB20190611B	10-Apr-2021	21:22:58.94	-79:23:51.3	6''.446×6''.446	0.0052	< 0.0155
FRB20190611B	05-Sep-2021	21:22:58.94	-79:23:51.3	6''.723×6''.723	0.0055	< 0.0164
FRB20191228A	06-Sep-2021	22:57:43.33	-29:35:38.8	5''.813×5''.813	0.0063	< 0.0189
FRB20220330	20-Jan-2023	18:17:52.83	-24:23:42.5	5''.746×5''.746	0.0120	< 0.0360
FRB20220330	01-Dec-2023	18:17:52.83	-24:23:42.5	5''.413×5''.413	0.0080	< 0.0241
FRB20220330	13-Jan-2024	18:17:52.83	-24:23:42.5	5''.728×5''.728	0.0089	< 0.0269
FRB20200430A	19-Apr-2021	15:18:49.55	+12:22:34.8	7''.283×7''.283	0.0058	< 0.0175
FRB20200430A	28-Jul-2021	15:18:49.55	+12:22:34.8	8''.583×8''.583	0.0056	< 0.0164
FRB20210117A	16-Dec-2022	22:39:55.015	-16:09:05.45	5''.185×5''.185	0.0068	< 0.0205
FRB20220105A	08-Jan-2023	13:55:12.81	+22:27:58.4	6''.350×6''.350	0.0065	< 0.0196
FRB20220222C	09-Feb-2023	13:35:37.06	-28:01:37.2	5''.382×5''.382	0.0059	< 0.0179
FRB20220501C	09-Nov-2023	23:29:31.00	-32:29:26.6	5''.441×5''.441	0.0056	< 0.0168
FRB20220717A	28-Dec-2023	19:33:13.0	-19:17:15.8	—	—	Calibration failed
FRB20220717A	02-Mar-2024	19:33:13.0	-19:17:15.8	5''.419×5''.419	0.0095	< 0.0284
FRB20220905A	12-Dec-2023	16:54:19.79	-20:04:16.2	5''.644×5''.644	0.0017	< 0.0052
FRB20230125D	18-Jun-2024	10:00:49.33	-31:32:41.1	6''.606×6''.606	0.0059	< 0.0179

**Table 3.** List of redshifts of the FRB as well as the optical counterpart.

Source name	Optical Counterpart	Ref. (Host)	X-ray counterpart	Host(As reported)
FRB20181112A	Yes(DESI-Legacy-survey)	<a href="#">Prochaska et al. (2019)</a>	No	Host galaxy
FRB20190608B	Yes (Pan-STARRS)	<a href="#">Bhandari et al. (2022)</a>	Yes (Chandra)	AGN(seyferts)
FRB20191001A	Yes (DESI-Legacy-survey )	<a href="#">Bhandari et al. (2020b)</a>	No	Radio galaxy
FRB20200906A	Yes (Pan-STARRS)	<a href="#">Bhandari et al. (2022)</a>	No	SF galaxy
FRB20210320C	Yes (Pan-STARRS)	<a href="#">Gordon et al. (2023)</a>	No	SF galaxy
FRB20210410D	Yes (DESI-Legacy-survey)	<a href="#">Caleb et al. (2023)</a>	No	Quiescent galaxy
FRB20210807D	Yes(Pan-STARRS)	<a href="#">Gordon et al. (2023)</a>	No	Quiescent galaxy
FRB20210912A	No	<a href="#">Marnoch et al. (2023)</a>	No	Unseen host galaxy
FRB20211127I	Yes (Pan-STARRS)	<a href="#">Gordon et al. (2023)</a>	No	SF galaxy
FRB20211212A	Yes (Pan-STARRS)	<a href="#">Gordon et al. (2023)</a>	No	Host galaxy
FRB20220501C	Yes (DESI-Legacy-survey)	<a href="#">Shannon et al. (2025)</a>	No	Host galaxy
FRB20220725A	Yes(DESI-Legacy-survey)	<a href="#">Shannon et al. (2025)</a>	No	host galaxy
FRB20220918A	Yes (DESI-Legacy-survey)	<a href="#">Shannon et al. (2025)</a>	No	LMC
FRB20221106A	Yes (Pan-STARRS)	<a href="#">Shannon et al. (2025)</a>	No	Host galaxy

the South African Radio Astronomy Observatory. In addition we acknowledge the ilifu cloud computing facility- [www.ilifu.ac.za](http://www.ilifu.ac.za).

## DATA AVAILABILITY

The data used in this work will be shared upon request.

Source name	Position in radio		$\Delta\theta_{FRB}$ ('')	Radio-Optical offsets		
	RA	Dec		$\Delta\theta_{Radio}$ ('')	$\Delta RA$ ('')	$\Delta Dec$ ('')
FRB20181112A	21:49:24.000	-52:58:09.859	6.5	6.6	5.51	-5.69
FRB20190608B	22:16:04.882	-7:53:55.556	2.49	0.18	-0.029	0.177
FRB20191001A	21:33:24.527	-54:44:54.598	1.23	0.59	0.553	0.212
FRB20200906A	3:33:59.033	-14:04:59.107	1.53	0.78	0.77	0.172
FRB20210320C	13:37:50.014	-16:07:22.510	1.54	1.9	1.684	0.837
FRB20210410D	21:44:19.969	-79:19:04.868	2.15	3.0	3.00	0.045
FRB20210912A	23:23:10.243	-30:24:19.732	2.57	—	—	—
FRB20210807D	19:56:52.920	-0:45:44.500	2.29	0.19	-0.075	-0.172
FRB20211127I	13:19:13.848	-18:50:18.900	3.96	1.65	1.62	0.34
FRB20211212A	10:29:24.290	1:21:38.800	1.92	1.19	1.065	-0.525
FRB20220501C	23:29:30.999	-32:29:26.584	0.020	0.43	0.404	0.154
FRB20220725A	23:33:15.631	-35:59:24.900	0.23	0.62	0.595	-0.174
FRB20220918A	1:10:22.186	-70:48:40.505	0.618	1.21	1.11	0.474
FRB20221106A	3:46:48.358	-25:34:19.300	13.37	12.6	8.059	9.69

**Table 4.** Summary of positional offsets. The table presents (i) the angular separation  $\Delta\theta_{FRB}$  between the radio sources and the FRB positions in arcseconds, and (ii) the offsets between the radio and optical source positions. The latter includes the angular separation  $\Delta\theta_{Radio}$  and the  $\Delta RA$  and  $\Delta Dec$  offset components in arcseconds.

Source name	Instrument	$m_r$ mag[AB]	Ref.	Optical-flux mJy	Radio-flux mJy	RO-ratio
FRB20181112A	DES(DECam)	21.68	1	0.0077	0.0662	0.93
FRB20190608B	DECaLS(DECam)	17.41	2,3	0.3945	0.0236	-1.22
FRB20191001A	DECaLS(DECam)	18.36	4	0.1644	0.1059	-0.19
FRB20200906A	DECaLS(DECam)	19.95	5	0.0380	0.1298	0.53
FRB20210320C	SOAR(Goodman)	19.47	3,6	0.0592	0.1260	0.33
FRB20210410D	SOAR(Goodman)	20.65	3,7	0.0200	0.0977	0.69
FRB20210912A	—	—	—	—	—	—
FRB20210807D	Pan-STARRS	17.17	3,6	0.4921	0.4970	0.00
FRB20211127I	SOAR(Goodman)	14.96	3,6	3.7673	0.5055	-0.87
FRB20211212A	SOAR(Goodman)	16.44	3,6	0.9639	0.3600	-0.43
FRB20220501C	—	—	—	—	—	—
FRB20220725A	—	—	—	—	—	—
FRB20220918A	—	—	—	—	—	—
FRB20221106A	—	—	—	—	—	—

**Table 5.** The optical photometry of FRB host galaxies detected by ASKAP/CRAFT from different imaging instruments. The AB- $m_r$  magnitude values in the  $r$ -band were obtained from the literature. References: (1) Prochaska et al. (2019), (2) Macquart et al. (2020), (3) Gordon et al. (2023), (4) Bhandari et al. (2020b), (5) Bhandari et al. (2020a), (6) James et al. (2022), (7) Caleb et al. (2023).

## REFERENCES

Afonso J., Georgakakis A., Almeida C., Hopkins A. M., Cram L. E., Mobasher B., Sullivan M., 2005, *ApJ*, **624**, 135

An T., Wang A., Huang Y.-C., Feng J.-P., Liu Y., Zhang Z., Dai Z.-G., 2025 ([arXiv:2508.05552](https://arxiv.org/abs/2508.05552))

Bhandari S., et al., 2020a, *ApJ*, **895**, L37

Bhandari S., et al., 2020b, *The Astrophysical Journal Letters*, **901**, L20

Bhandari S., et al., 2022, *The Astronomical Journal*, **163**, 69

Bhandari S., et al., 2023, *The Astrophysical Journal*, **948**, 67

Brown A. G., et al., 2021, *Astronomy & Astrophysics*, **649**, A1

Bruni G., et al., 2024, *nat*, **632**, 1014

Bruni G., et al., 2025, *aap*, **695**, L12

Burrows D. N., et al., 2005, *Space science reviews*, **120**, 165

Caleb M., et al., 2023, *Monthly Notices of the Royal Astronomical Society*, **524**, 2064

Chatterjee S., et al., 2017, *Nature*, **541**, 58–61

Chibueze J. O., et al., 2022, *MNRAS*, **515**, 1365

Chittidi J. S., et al., 2021, *The Astrophysical Journal*, **922**, 173

Dai Z. G., Wang J. S., Yu Y. W., 2017, *ApJ*, **838**, L7

Dey A., et al., 2019, *The Astronomical Journal*, **157**, 168

Dong Y., et al., 2024, *The Astrophysical Journal*, **973**, 133

Eftekhari T., Berger E., 2017, *apj*, **849**, 162

Eftekhari T., et al., 2021, *The Astrophysical Journal*, **912**, 21

Flewelling H. e., et al., 2020, *The Astrophysical Journal Supplement Series*, **251**, 7

Gordon A. C., et al., 2023 ([arXiv:2302.05465](https://arxiv.org/abs/2302.05465))

Heintz K. E., et al., 2020, *The Astrophysical Journal*, **903**, 152

Heywood I., 2020, oxkat: Semi-automated imaging of MeerKAT observations, *Astrophysics Source Code Library*, record ascl:2009.003

Heywood I., et al., 2022, *mnras*, **509**, 2150

Ibik A. L., et al., 2024 ([arXiv:2409.11533](https://arxiv.org/abs/2409.11533)), <https://arxiv.org/abs/2409.11533>

James C. W., et al., 2022, *MNRAS*, **516**, 4862

Kashiyama K., Ioka K., Mészáros P., 2013, *The Astrophysical Journal*, **776**, L39

Kenyon J. S., Smirnov O. M., Grobler T. L., Perkins S. J., 2018, *MNRAS*, **478**, 2399

Kirsten F., et al., 2024, *Nature Astronomy*, **8**, 337

Law C. J., Connor L., Aggarwal K., 2022, *The Astrophysical Journal*, **927**, 55

Lindsay S. N., et al., 2014, *mnras*, **440**, 1527

Lorimer D. R., Bailes M., McLaughlin M. A., Narkevic D. J., Crawford F., 2007, *Science*, **318**, 777

Macquart J.-P., et al., 2020, *Nature*, **581**, 391–395

Maddox S. J., Sutherland W. J., Efstathiou G., Loveday J., 1990, *mnras*, **243**, 692

Magliocchetti M., Maddox S., 2002, *Monthly Notices of the Royal Astronomical Society*, **330**, 241–250

Marcote B., et al., 2017, *ApJ*, **834**, L8

Margalit B., Berger E., Metzger B. D., 2019, *The Astrophysical Journal*, **886**, 110

Marnoch L., et al., 2023, *Monthly Notices of the Royal Astronomical Society*, **525**, 994–1007

McMullin J. P., et al. 2007, in *Astronomical Data Analysis Software and Systems XVI*. p. 127

Moroianu A. M., et al., 2025 ([arXiv:2509.05174](https://arxiv.org/abs/2509.05174)), <https://arxiv.org/abs/2509.05174>

Nimmo K., et al., 2022, *The Astrophysical Journal Letters*, **927**, L3

Niu C.-H., et al., 2022, *Nature*, **606**, 873–877

Offringa A. R., et al., 2014, *MNRAS*, **444**, 606

Orosz G., Frey S., 2013, *aap*, **553**, A13

Pastor-Marazuela I., et al., 2025 ([arXiv:2507.05982](https://arxiv.org/abs/2507.05982))

Popov S. B., Postnov K. A., 2013, *arXiv e-prints*, p. arXiv:1307.4924

Prochaska J. X., et al., 2019, *Science*, **366**, 231–234

Rajwade K. M., et al., 2024 ([arXiv:2407.02173](https://arxiv.org/abs/2407.02173))

Ravi V., et al., 2022, *Monthly Notices of the Royal Astronomical Society*, **513**, 982–990

Shannon R. M., et al., 2025, *Publications of the Astronomical Society of Australia*, **42**

The CHIME/FRB Collaboration et al., 2023, *The Astrophysical Journal*, **947**, 83

Totani T., 2013, *Publications of the Astronomical Society of Japan*, **65**, L12

Wang X.-W., et al., 2025 ([arXiv:2508.15615](https://arxiv.org/abs/2508.15615))

Weisskopf M., et al. 2002, *Publications of the Astronomical Society of the Pacific*, **114**, 1

Whittam I. H., et al., 2023 ([arXiv:2310.17409](https://arxiv.org/abs/2310.17409)), <https://arxiv.org/abs/2310.17409>

Wright E. L., et al., 2010, *The Astronomical Journal*, **140**, 1868

Yamanaka I., Hatsukade B., Egusa F., Hashimoto T., Niino Y., Hsu T.-Y., Kaneko H., Kohno K., 2024 ([arXiv:2407.01889](https://arxiv.org/abs/2407.01889))

Yamasaki S., Totani T., Kiuchi K., 2018, *Publications of the Astronomical Society of Japan*, **70**, 39

Yang Y.-P., Li Q.-C., Zhang B., 2020, *apj*, **895**, 7

## APPENDIX A: FRB PROPERTIES

Table A1 lists all the FRB names and their key properties discovered by ASKAP/CRAFT and MeerTRAP.

### A1 A brief overview of individual MeerKAT detections

This section gives a brief overview of 14 radio sources detected by MeerKAT. We provide details of some properties of the emission and their hosts.

#### A1.1 FRB20181112A field

This is a two-epoch observation. [Prochaska et al. \(2019\)](#) studied the host galaxy of the FRB in detail and identified a bright foreground galaxy close to the host galaxy. The foreground galaxy consists of a massive halo of gas, which acts as a reservoir of material that may fuel star formation in the future. Both the foreground and the host galaxies have been identified in optical wavelengths in the DESI-legacy-survey, where the northern optical source is the foreground, while the southern source is the host galaxy. Therefore, the detection of continuum radio emission is probably stronger for the foreground galaxy compared to the host galaxy. No X-ray source was found.

#### A1.2 FRB20190608B field

Two epochs were observed toward this FRB position and there is a detection in both. The host galaxy of FRB20190608B has been studied in some detail ([Chittidi et al. 2021](#); [Bhandari et al. 2022](#)), thus the FRB is localised to a star-forming spiral galaxy that contains an AGN at its centre. We found an optical FITS image in the Pan-STARRS catalog (Figure A2) indicating an optical source coinciding with the detected radio source. An X-ray FITS image was found in the *Chandra* archive. There seems to be a bright X-ray excess spatially coinciding with the radio source position. It is plausible that the AGN at the centre of the host galaxy may be responsible for the radio and X-ray emission.

#### A1.3 FRB20191001A field

The FRB20191001A position was observed for two epochs, and there is a detection in both epochs. The radio emission shows an interesting, extended morphology. [Yamanaka et al. \(2024\)](#) used ALMA to spatially resolve this source into two components, which are two spiral galaxies with a possibility of them merging. The FRB is localised on the north of the left spiral galaxy (cf. Figure A1). The optical FITS image of these galaxies was found in the DESI legacy survey. The X-ray FITS image from the *Swift* catalog, however, indicates that there is no detection at the FRB and host galaxy position (Figure A4). The detailed properties of a host galaxy are presented in [Heintz et al. \(2020\)](#). [Bhandari et al. \(2020b\)](#) used Australia Telescope Compact Array (ATCA) data to search for a compact PRS that is associated with the FRB. They detected low-level diffuse radio emission, however, they did not find a compact PRS above the flux density of  $15\mu$ Jy.

#### A1.4 FRB20200906A field

This is a single-epoch observation. We found an optical FITS image in the Pan-STARRS catalog indicating an elongated source, and [Bhandari et al. \(2022\)](#) reported it as a star-forming galaxy. However,

no X-ray source coinciding with the radio emission was found in the *Chandra* catalog.

#### A1.5 FRB20210410D field

Two epochs were observed at this FRB position, with a detection in both. The host galaxy of FRB20210410D has been studied by ([Caleb et al. 2023](#)), where the FRB is localised to the southeast of the host galaxy. [Caleb et al. \(2023\)](#) reported that persistent emission close to the FRB was not observed consistent with the position of the galaxy using MeerKAT. By visual inspection, the peak of the radio source is offset from the centre of the optical source found in the DESI legacy survey catalog. No X-ray FITS images were found in the archives.

#### A1.6 FRB20210912A field

This is a single-epoch observation. ([Marnoch et al. 2023](#)) did not find a host galaxy, despite deep optical ( $R > 26.7$  mag) and infrared (to  $K_s > 24.9$  mag) follow-up with the European Southern Observatory's Very Large Telescope (ESO VLT). We found no optical source spatially coinciding with the detected continuum radio emission. Thus, there is no redshift information on the FRB and the radio source. The radio emission could be emitted by a source that is highly redshifted or it could be an obscured galaxy at the optical wavelength.

#### A1.7 FRB20210807D field

This is a single-epoch observation at the FRB position. An optical FITS image from the DESI-legacy-survey reveals a spatially-coincident source with the radio emission. [Gordon et al. \(2023\)](#) reported it as a quiescent galaxy. We did not find an X-ray source in the archival catalogs coinciding with the detected radio source.

#### A1.8 FRB20211127I field

This is a single-epoch observation, and the optical and X-ray FITS images spatially coinciding with the radio emission's position were found in Pan-STARRS and *Chandra*, respectively. The optical counterpart shows a spiral galaxy that was reported to be a star-forming galaxy by [Gordon et al. \(2023\)](#).

#### A1.9 FRB20211212A field

This is a single-epoch observation. We found an optical source that spatially coincides with the radio emission in the Pan-STARRS catalog. There does not seem to be a significant X-ray excess from the *Chandra* catalog coinciding with the radio emission. [Gordon et al. \(2023\)](#) studied the host galaxy of this FRB, presenting the photometric and spectrometric observations of the host.

#### A1.10 FRB20210320C field

This is a single-epoch observation. An optical FITS image was found in Pan-STARRS. [Gordon et al. \(2023\)](#) reported that it is a star-forming galaxy. No X-ray source coinciding with this position was found in the archival catalogs.

#### A1.11 FRB20220501C field

This FRB position was observed for three epochs. There is no detection in the first epoch, however, there is a detection in the second and third epochs, and this suggests flux variability. The variability of these three epochs is of day-timescales, since we observed this field on 9, 25, and 26 November (see Table 1 and 2). The flux significantly decreases (the radio source is 9 times fainter in third epoch compared to the second epoch) as though the source is fading away. The variability could be as a result of intrinsic variability or it could be the result of scintillation effects. Therefore, more data are required to study this source.

There is no detailed study of the host (optical source) of FRB20220501C in the literature because it is not catalogued. However, there is a faint optical source from the DESI legacy survey spatially coinciding with the detected radio emission and FRB position and there is a bright ( $V = 11.6$  magnitude) star located  $15''$  from this optical source. The Set of Identifications, Measurements, and Bibliography for Astronomical Data (SIMBAD) database (<https://simbad.u-strasbg.fr/simbad/sim-fcoo>) did not identify nor classify the optical source. No X-ray FITS images were found in the archival catalogues that are spatially associated with the radio source. A detailed study on the host of this FRB is encouraged.

#### A1.12 FRB20220725A field

This is a single-epoch observation, and a spatially-coincident optical source was found in DESI-legacy-survey. [Shannon et al. \(2025\)](#) claimed that the FRB coincides with the catalogued galaxy WISEA J233315.68-355925.0 ([Maddox et al. 1990](#)), with an optical magnitude of  $b_J = 19.0$ . No coinciding X-ray image was found.

#### A1.13 FRB20220918A field

This is a single-epoch observation, with the radio source exhibiting an interesting morphology. This source has a tail (which may perhaps be ejected material from the centre). A high-resolution observation may reveal multiple sources/clumps in the region. There is no detailed study on the host of FRB20220918A in the literature. An optical FITS image was found in DESI legacy survey, and SIMBAD classifies the optical source as the Small Magellanic Cloud (SMC). This raises an intriguing possibility that the radio continuum emission may perhaps be associated with the SMC. Interestingly, the FRB is at the centre of both the radio and optical sources. We could not find X-ray FITS images in the archives coinciding with the radio emission.

#### A1.14 FRB20221106A field

The FRB20221106A position was observed for three epochs, and there is a detection in all three. There is a hint of variability in the source morphology and peak flux. We found an optical source spatially coinciding with the radio emission (with high peak flux, from the second epoch) in the DESI legacy survey catalogue (Figure A1). [Shannon et al. \(2025\)](#) claimed that the galaxy WISEA J034649.07-253411.7 with an optical magnitude of  $b_J = 19.5$  ([Maddox et al. 1990](#)) coincides with the FRB position. There are no other recent studies on this host galaxy. Therefore, the host galaxy cannot be identified. SIMBAD suggests that it is a star cluster. The peak of the radio source is offset from the centre of the optical source. No X-ray FITS images were found in the archival catalogues.

**Table A1.** List of FRB name, dispersion measure (DM), the redshift and where it is obtained and also the positions in right ascension and declination taken from ASKAP/CRAFT and MeerTRAP. We also indicate which is a repeating source.

Source name	Ref.	DM pc/cm <sup>-3</sup>	<i>z</i>	RA	DEC	Repeater?	Instrument
FRB20181112A	(Prochaska et al. 2019)	589.0	0.4755	21:49:23.63	-52:58:15.4	N	ASKAP
FRB20190102C	(Macquart et al. 2020)	364.5	0.2912	21:29:39.76	-79:28:32.5	N	ASKAP
FRB20190608B	(Macquart et al. 2020)	339.5	0.1178	22:16:04.77	-07:53:53.7	N	ASKAP
FRB20190611B	(Macquart et al. 2020)	322.2	0.3778	21:22:58.94	-79:23:51.3	N	ASKAP
FRB20191001A	(Bhandari et al. 2020b)	506.92	0.234	21:33:24.37	-54:44:51.4	N	ASKAP
FRB20191228A	(Bhandari et al. 2022)	297.5	0.2432	22:57:43.33	-29:35:38.8	N	ASKAP
FRB20200430A	(Heintz et al. 2020)	380.1	0.1608	15:18:49.55	+12:22:34.8	N	ASKAP
FRB20200906A	(Bhandari et al. 2022)	577.8	0.3688	3:33:58.94	-14:04:59.9	N	ASKAP
FRB20210117A	(Bhandari et al. 2023)	730	0.2145	22:39:55.015	-16:09:05.45	N	ASKAP
FRB20210320C	(James et al. 2022; Gordon et al. 2023)	384.8	0.2797	13:37:50.09	-16:07:21.7	N	ASKAP
FRB20210410D	(Caleb et al. 2023)	578.8	0.1415	21:44:20.63	-79:19:05.6	N	MeerTRAP
FRB20210807D	(James et al. 2022; Gordon et al. 2023)	251.9	0.1293	19:56:53.14	-0:45:44.5	N	ASKAP
FRB20210912A	(Marnoch et al. 2023)	1234.5	–	23:23:10.44	-30:24:20.1	N	ASKAP
FRB20211127I	(James et al. 2022; Gordon et al. 2023)	234.83	0.0469	3:19:14.08	18:50:16.7	N	ASKAP
FRB20211212A	(James et al. 2022; Gordon et al. 2023)	206	0.0707	10:29:24.16	1:21:37.7	N	ASKAP
FRB20220105A	(Gordon et al. 2023)	583	0.2785	13:55:12.81	+22:27:58.4	N	ASKAP
FRB20220222C	(Pastor-Marazuela et al. 2025)	1071.2	0.853	13:35:37.06	-28:01:37.2	N	MeerTRAP
FRB20220330	–	900	–	18:17:52.83	-24:23:42.5	N	MeerTRAP
FRB20220501C	(Shannon et al. 2025)	449.5	0.381	23:29:31.00	-32:29:26.6	N	ASKAP
FRB20220717A	(Rajwade et al. 2024)	637	0.36295	19:33:13.0	-19:17:15.8	N	MeerTRAP
FRB20220725A	(Shannon et al. 2025)	290.4	0.1926	23:33:15.65	-35:59:24.9	N	ASKAP
FRB20220905A	(Rajwade et al. 2024)	800.6	–	16:54:19.79	-20:04:16.2	N	MeerTRAP
FRB20220918A	(Shannon et al. 2025)	656.8	0.491	01:10:22.11	-70:48:41.0	N	ASKAP
FRB20221106A	(Shannon et al. 2025)	343.8	0.2044	3:46:49.09	-25:34:10.5	N	ASKAP
FRB20230125D	(Pastor-Marazuela et al. 2025)	640.08	0.3265	10:00:49.33	-31:32:41.1	N	MeerTRAP

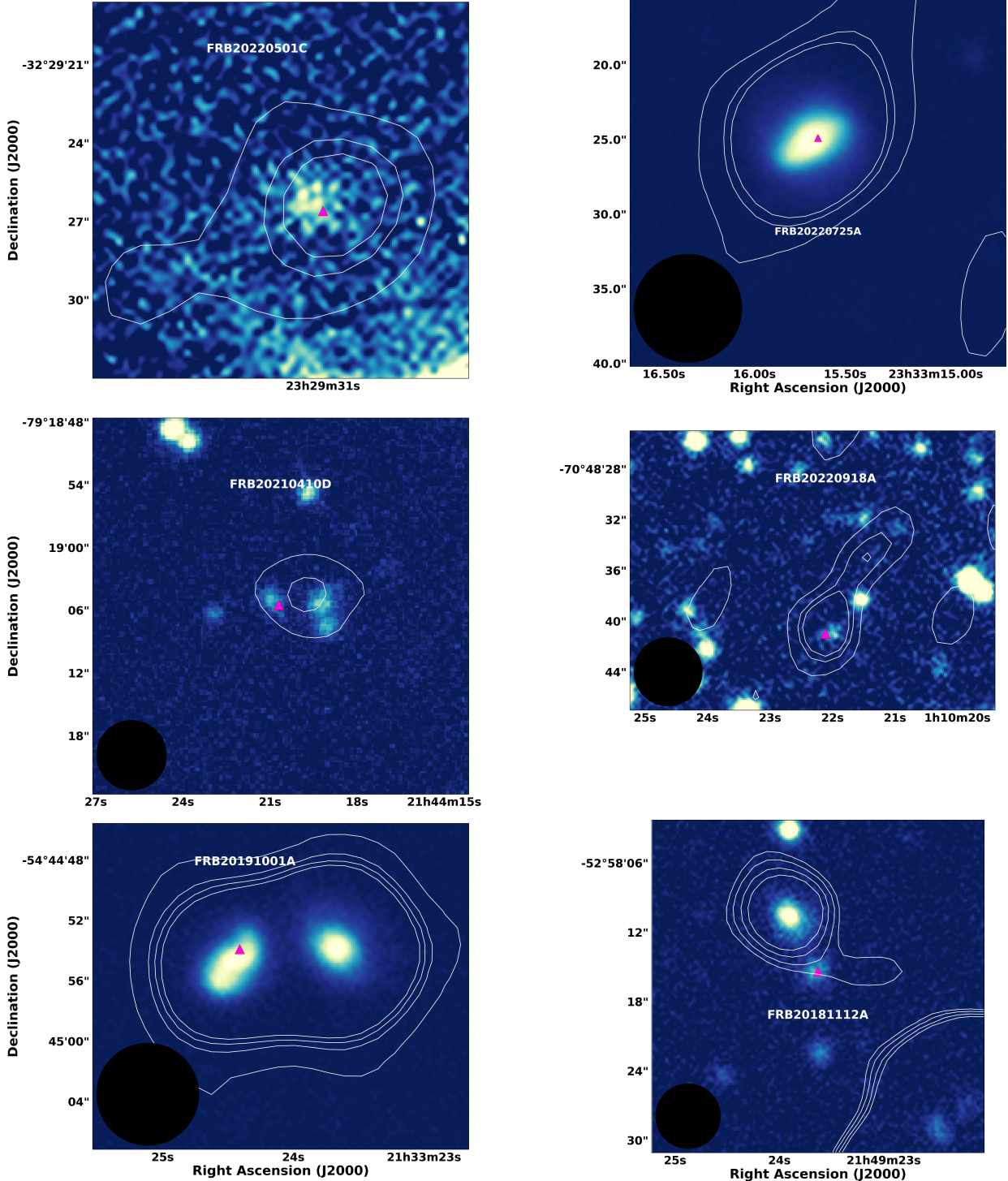


**Figure A1.** Optical fields with the MeerKAT radio contours overlaid. The background is the DESI-Legacy survey *grz*-band optical flux and the white contours represent the MeerKAT radio emission corresponding to 3, 6, 12, 24 times the rms of the image. The magenta triangle is the position of the FRB and black circle in the bottom left corner represents the size of the MeerKAT beam.

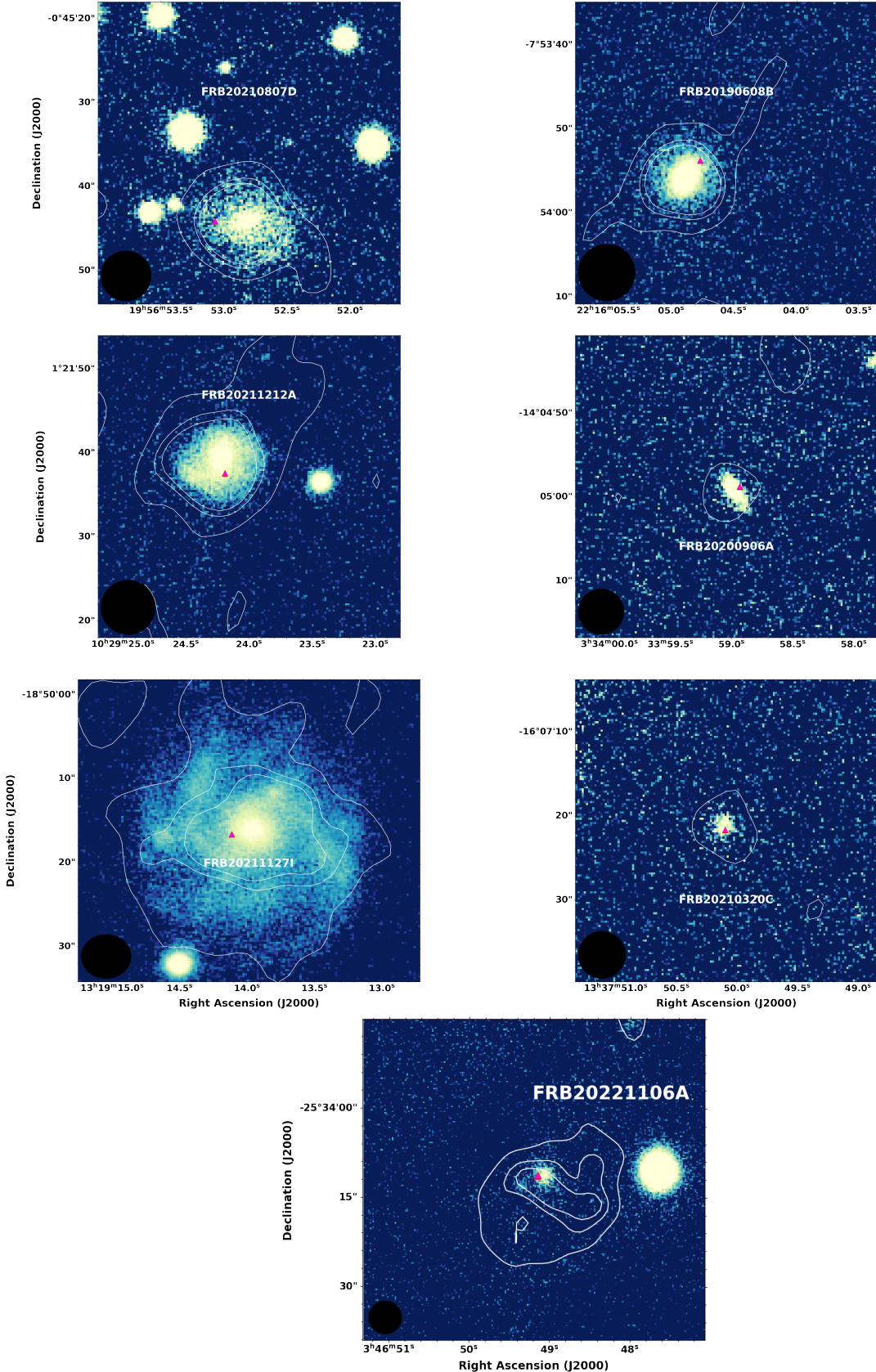


**Figure A2.** Optical fields with the MeerKAT radio contours overlaid. The background is the Pan-STARRS  $g$ -band optical flux and the white contours represent the radio emission corresponding to 3, 6, 12, 24 times the rms of the image. The magenta triangle is the position of the FRB and black circle in the bottom left corner represents the size of the MeerKAT beam.

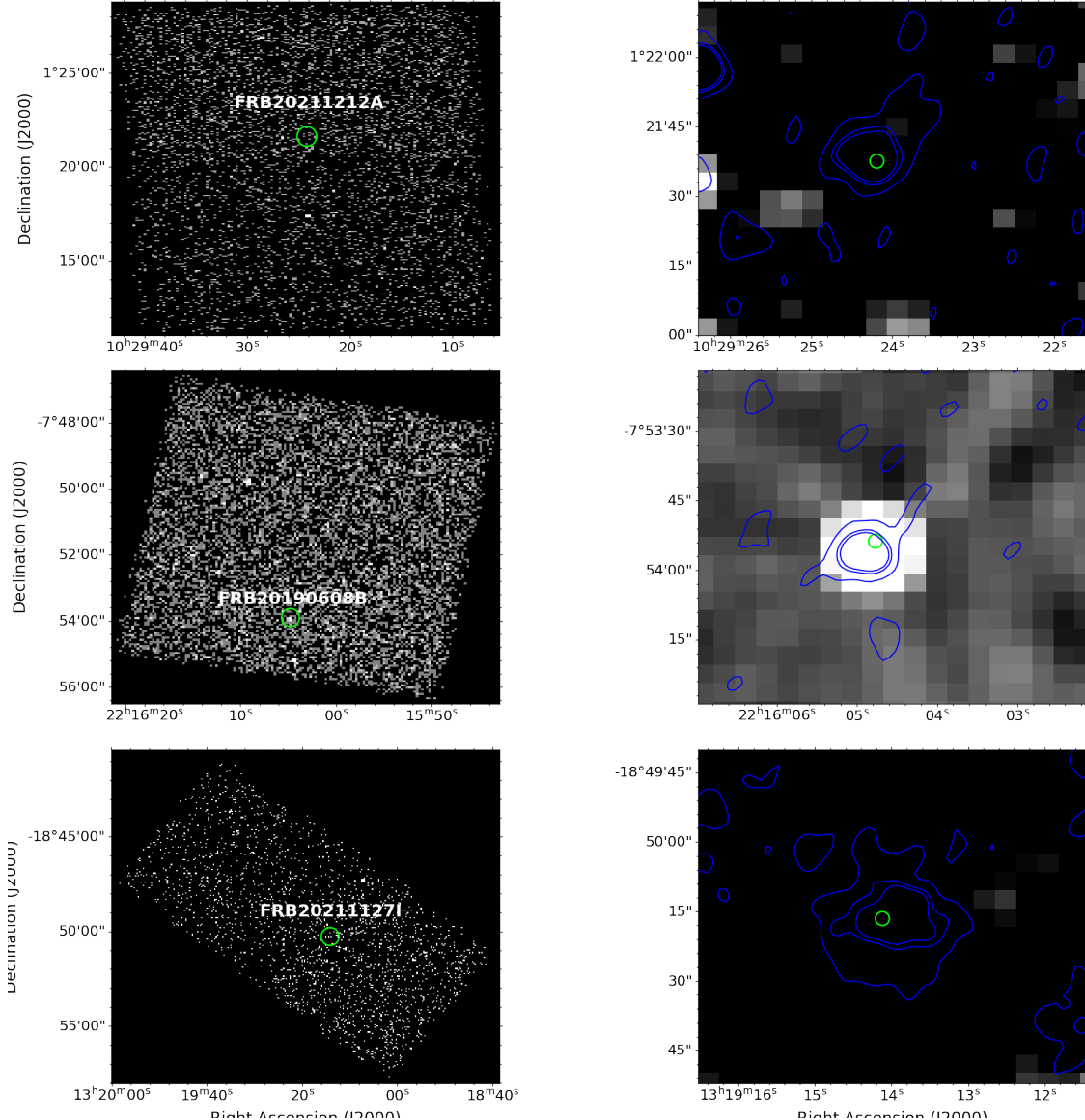


**Figure A3.** The *Chandra* X-ray images coinciding with FRB positions. *Left:* The green circle represents the FRB position. *Right:* The zoomed image close to the FRB position. The blue contours represent the radio emission corresponding with 3, 6, 12, 24 times the rms of the image, and the green circle is the FRB position.

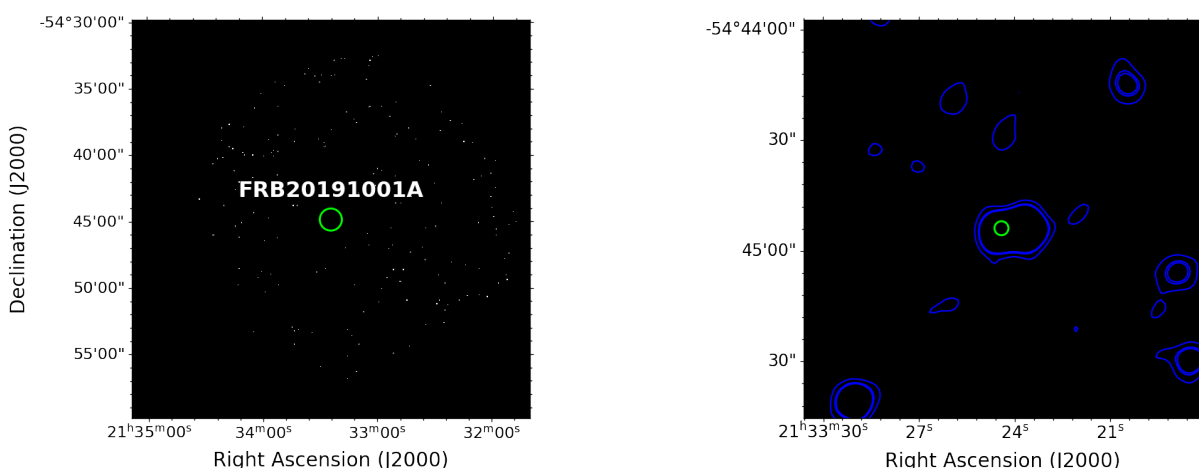


**Figure A4.** The *Chandra* X-ray images coinciding with FRB positions. *Left:* The green circle represents the FRB position. *Right:* The zoomed image close to the FRB position. The blue contours represent the radio emission corresponding with 3, 6, 12, 24 times the rms of the image, and the green circle is the FRB position.